Investigating the effect of polydispersity on the dynamics of multiphase flows using computational fluid dynamics tools

Francesco Neglia [a,*], Roberto Sulpizio [a], Fabio Dioguardi [a], Damiano Sarocchi [b]

[a] Dipartimento di Scienze della Terra e Geoambientali, Universita` di Bari, Bari, Italy
[b] Instituto de Geologia, Facultad de Ingeneria, Universidad Auto´noma de San Luis Potosi, San Luis Potosì, M´exico

A B S T R A C T

Granular flows consist of discrete macroscopic particles. If they are non-cohesive, their status is determined by the interaction of particle-particle frictional forces, external boundaries and gravity. In particular, the under- standing of the transport mechanisms of granular materials is of paramount importance for the characterization of volcanic granular flows and for hazard assessments associated with these flows. In order to investigate dy- namics of these kinds of flows, we replicated large-scale experiments with multiphase computational fluid dy- namic (CFD) simulations using the Two-Fluid Model approach, with an emphasis on the polydispersity effect on the flow behaviour. The CFD simulations were run using the software MFIX. The present work consists of: 1) investigations on the drag force relationships implemented in MFIX; 2) applications of MFIX to replicate large- scale experiments on volcanic dry granular flows sliding on an inclined channel; 3) comparisons between experimental and simulated data with particular emphasis on the velocity of the granular flow front. Simulations on polydisperse granular flows demonstrated the simulated flows capability to replicate segregation dynamics active in real granular flows, and the polydispersity effects on velocities and shapes of granular flows. The non- uniformity of solid phases highly affects the dynamic of the whole flow and results in a better agreement between simulated and experimental flow velocities than the simplest monodisperse particles systems. In particular, the greater the number of the solid phases, the lower the velocity of granular flows and the mean square error, which decreases by ca. 50%

1. Introduction

Volcanic granular flows are gravity-driven mixtures generated by gravitational collapse of summit lava domes and of eruptive columns generated during explosive eruptions. The community's interest about these volcanic events is justified by the hazard posed by their capability to propagate over kilometric distances, affecting thereby very extensive areas. A better understanding of dynamics ruling the mobility of volcanic granular flows is fundamental to predict their run-out distances, velocities and dynamic pressures. The solid mixtures constituting volcanic granular flows like debris flows, pyroclastic density currents and debris avalanches are usually polydisperse, with a continuous grain-size distribution from coarse to fine sizes and with a wide range of densities (Iverson, 1997; Sarocchi et al., 2011; Sulpizio et al., 2016; Lube et al., 2020). Furthermore, movement of polydisperse particulate mixtures are involved in a wide range of industrial processes as fluidised beds, pneumatic transport, generic particle flows in and from hoppers, silos and conveyor belts (Cleary and Sawley, 2002).

In volcanic phenomena involving polydisperse mixtures, the fine-grained particles play a crucial role in the flow dynamics, promoting high pore fluid pressures that maintain the fluidization state (Druitt, 1998; Roche et al., 2005, 2010). As well known in multiphase flow dynamics, for a particle settling in a fluid, the finer the particle's size, the lower the settling velocity, which implies a greater facility for escaping gas phases to support finer solid phases. Furthermore, in fine-rich grain-sizes the smaller particles fill the inter-granular voids of the larger ones inducing low porosities, which, according to the classic Ergun equation (Ergun, 1952), promotes favorouble conditions for the fluidization phenomenon (Sulpizio et al., 2014). Hence, the fine particles induce a porosity decrease in the granular flows and have greater chance of being transported to the top flow by the escaping fluids, while the grains having settling velocities too high to be fluidised are subjected to downward segregation. In granular flow regimes, the fluidisation state is not reached, and the fine-grained particles concentrate at the

https://doi.org/10.1016/j.ijmultiphaseflow.2023.104558

Table 1
List of symbols with description and physical dimension.

Symbol	Description	Dimension
A	constant of Eq. $P^* = A(\varepsilon^*_g - \varepsilon_g)^{10}$	Pa
C_f	friction coefficient between the solid phases	-
C_1	segregation sloping coefficient	s m^{-2}
d	particle diameter	M
e_p	restitution coefficient for the particle-particle collision	-
g	gravitational acceleration	m s^{-2}
g_0	radial distribution function	-
I	unit tensor	-
I_{gm}	momentum transfer from fluid phase to m^{th} solid phase	kg m^{-2} s^{-1}
I_{ml}	momentum transfer from m^{th} to l^{th} solid phase	kg m^{-2} s^{-1}
P	Pressure	Pa
r	term of Yu and Standish relation (Eq. 14)	-
t	Time	s
U	velocity	m s^{-1}

Greek symbol	Description	Dimension
α_{sml}	drag coefficient between m^{th} and l^{th} solid phase	kg m^{-3} s^{-1}
β_{gm}	drag coefficient between fluid and solid phase	kg m^{-3} s^{-1}
δ_{int}	internal friction angle of the granular material	◦ (degree)
δ_w	wall friction angle of the granular material	◦ (degree)
ε	volume concentration	-
θ	granular temperature	m^2 s^{-2}
μ	viscosity	Pa s
μ_b	bulk viscosity	Pa s
ρ	density	kg m^{-3}
τ	stress tensor	Pa
ϕ	specularity coefficient	-

Subscripts	
g	fluid phase
m	solid phase m^{th}
s	solid phase

Superscript	
*	maximum packing
f	frictional
k	kinetic

base of the flow due to processes of kinetic sieving and kinematic squeezing affecting the larger particles (Le Roux, 2003; Sulpizio et al., 2014). This means they underwent most of the frictional processes occurring at the contact between the flow and the topography. For these reasons, it is very important to investigate how the particles size distribution of the granular media affect natural or experimental granular flows, with particular emphasis on the fine-grained phases.

This work deals with the study of the influence of polydispersity of particle size on computational fluid dynamics (CFD) simulations of multiphase granular flows, highlighting the solids-solids drag force's role in segregation processes and the relationship between the number of solid phases and the flow propagation dynamics. It represents the prosecution of the work of Neglia et al. (2022), which instead focused on the effect of the selected wall-solid phase boundary condition on the dynamics of the granular flow. In that work, the simulated granular mixtures were approximated by purely monodisperse particles systems, thus neglecting the polydispersity effects on the simulations results and the processes induced by non-uniformity of the particle sizes. The results of Neglia et al. (2022) were used to optimally set-up the boundary conditions and inputs of the numerical simulation presented in this works, which take into account the complexity of approximating the granular mixtures as a polydisperse particle system.

To achieve this goal, the multiphase CFD simulation tool MFIX (http://mfix.netl.doe.gov/) (Syamlal et al., 1993) (version 20.2.1) was used. MFIX provides various models that treat multiphase flows simulations with different approaches, e.g. the Discrete Element Method (DEM) (Cundall and Strack, 1979 Garg et al., 2012; Li et al., 2012) and the Two-Fluid Model (TFM) (Campbell, 1990; Lun et al., 1984). As already discussed in Neglia et al. (2022), the more feasible approach for granular flows involving large numbers of particles is the TFM approach, which treats the gas and solid phase as interpenetrating continua whose motion is ruled by the Navier-Stokes Equation. Since the motion of individual particles is not directly solved in the TFM, closure relationships for modelling the momentum coupling between the solid and the fluid phase, the particle-particle momentum exchange and the solid-wall interactions. When using this approach to simulate polydisperse systems, each class of particle is treated as a separate solid phase, hence resulting in the conservation equations being solved for each solid phase. The presence of multiple solid phases leads to additional terms in momentum conservations equations of the TFM, namely terms accounting for the momentum transfer between the different solid phases, which in turn depend on the solid-solid interactions (e.g. collisions). The latter is given by the drag force experienced between the solid phases and is difficult to model (Lu et al., 2018). The problem of the drag force modelling was addressed by Syamlal et al. (1987) who developed a particle-particle drag term using the kinetic theory of granular flow.

The current work consists of: 1) an investigation on the drag force relationships implemented in MFIX by means of sensitivity analysis of simulated bidisperse granular mixtures on different flow parameters; 2) an application of MFIX to replicate three large-scale experiments on volcanic dry granular flows sliding on an inclined channel (including the experiment already analysed in Neglia et al. (2022)); and, 3) a comparison between experimental and simulated data obtained from simulations of mono-, bi- and tridisperse granular mixtures, analysing the difference in the flow parameters with particular emphasis on the velocity of the granular flow front. Input and output data of MFIX reported in the current paper are available in Zenodo (10.5281/zenodo.7818452). The Zenodo repository includes an input files directory,

where every file is identified by means of an ID, a table listing the input files ID and the corresponding simulation parameters and finally an output directory containing the output data used to develop the graphs reported in the manuscript.

2. Two-fluid model and drag force equations implemented in MFIX code

In the TFM the gas and solid phase are treated as interpenetrating continua, whose motion is solved using the Eulerian-Eulerian approach. Flow variables are volume-averaged over a region named control volume (CV), which is large if compared with particle size but small compared with the scale of macroscopic variations inside the flow domain (Anderson and Jackson, 1967). For each phase the Navier-Stokes equations for the conservation of mass, momentum and granular energy are solved, with constitutive equations accounting for the interphase interactions. In this work, the flow is considered isothermal and the energy conservation equations are not reported.

The conservation equations of mass for gas and m^{th} solid phase are:

$$\frac{\partial\left(\varepsilon_g\rho_g\right)}{\partial t}+\nabla\cdot\left(\varepsilon_g\rho_g U_g\right)=0 \tag{1}$$

$$\frac{\partial(\varepsilon_{sm}\rho_{sm})}{\partial t}+\nabla\cdot(\varepsilon_{sm}\rho_{sm}U_{sm})=0 \tag{2}$$

where ε is the volume concentration, ρ is the density, U is the velocity vector and the subscripts s and g denote the solid and fluid phase, respectively. All symbols are listed in Table 1. The first term on the left-hand side states for the mass change rate per unit volume and the second one is the convective mass flux. Potential sinks and sources due to phase changes and chemical reactions are neglected.

The conservation equation of the granular energy is given by:

$$\frac{3}{2}\rho_{sm}\left(\frac{\partial(\varepsilon_{sm}\theta_m)}{\partial t}+\nabla\cdot(\varepsilon_{sm}\theta_m U_{sm})\right)=-\nabla\cdot q+\tau_{sm}:\nabla U_{sm}-\gamma_{\theta_m}+\varphi_{gm}+\sum_{l=1,l\neq m}^{M}\varphi_{lm} \tag{3}$$

where θ is the granular temperature, which is proportional to the mean quadratic fluctuating velocity due to the random motion of the particles, q is the diffusive flux of granular energy, γ_θ represents the granular energy dissipation due to inelastic collisions, φ_{gm} is the transferred granular energy between gas and the m^{th} solids phase and φ_{lm} accounts for the transferred granular energy between the m^{th} and l^{th} solid phase. The terms on the left-hand side are the rate of change and the advection of the granular temperature, respectively. The first term on the right-hand side is the diffusive transport of granular energy, the second term is the net rate of granular energy produced by shear and the third term represent dissipation of granular energy.

The conservation equations of momentum for the gas and solid phase are reported below:

$$\frac{\partial\left(\varepsilon_g\rho_g U_g\right)}{\partial t}+\nabla\cdot\left(\varepsilon_g\rho_g U_g U_g\right)=\nabla\cdot\tau_g+\varepsilon_g\rho_g g-\sum_{m=1}I_{gm} \tag{4}$$

$$\frac{\partial(\varepsilon_{sm}\rho_{sm}U_{sm})}{\partial t}+\nabla\cdot(\varepsilon_{sm}\rho_{sm}U_{sm}U_{sm})=\nabla\cdot\tau_{sm}+\varepsilon_{sm}\rho_{sm}g+I_{gm}+\sum_{l=1,l\neq m}I_{lm} \tag{5}$$

here g is the gravitational acceleration, τ_g and τ_{sm} are the fluid and solid phase stress tensors, respectively, I_{gm} and I_{ml} represent the transferred momentum between the gas phase and the m^{th} solid phase and between the different solid phases, respectively, and subscripts m and l indicate the m^{th} and l^{th} solid phase. The first term on the left-hand side of Eqs. 4 and 5 accounts for the net rate of momentum variation and the second states for the net rate of momentum transported by convection. The first and second term on the right -hand side represent forces due to the stress tensor and the body forces, respectively.

τ_{sm} is described by means of kinetic and frictional components, where the kinetic-collisional stress is calculated applying the kinetic theory to the granular systems (Boyle and Massoudi, 1989) and the frictional term is computed using the rigid-plastic rheological model proposed by Schaeffer (1987). MFIX combines the kinetic and the frictional theories by considering a "switch" value represented by is the void volume concentration at the maximum packing ε_g^* (Syamlal et al., 1993):

$$\tau_{sm}=\begin{cases}-P_{sm}^f I+2\mu_{sm}^f S & \varepsilon_g\leq\varepsilon_g^*\\ \left(-P_{sm}^k+\eta\mu_b\nabla\cdot v_s\right)I+2\mu_{sm}^k S & \varepsilon_g>\varepsilon_g^*\end{cases} \tag{6}$$

where P_{sm}^f and P_{sm}^k are the solid pressure for the frictional and kinetic-collisional regime, respectively, I is the unit tensor, S is the strain rate tensor, $\eta=(1+e_p)/2$ with e_p being the particle-particle restitution coefficient, μ_{sm}^k and μ_{sm}^f are the kinetic and solid viscosity, respectively, and μ_b is the bulk viscosity. e_p is proportional to the fraction of the original kinetic energy that is restored to the particles after collision. The greater the restitution coefficient, the lower the dissipation rate of the inelastic collisions. P_{sm}^f can be calculated using the models proposed by Schaeffer (1987) and by Srivastava and Sundaresan (2003). The former was proposed for a plastic flow of granular medium occurring when the solid volume concentration exceeds ε_g^* and uses an arbitrary function to prevent unphysically large solid volume concentration (Gera et al., 2004) and to take a certain amount of compressibility in the solid phase into account (Pritchett et al., 1978). The latter, also named "Princeton model", was implemented in MFIX more recently, and starts from the quasi-static model proposed by Schaeffer (1987) modifying it to consider strain rate fluctuations associated to the shear layers that decrease the shear stress in the granular material (Savage, 1998). Using the Princeton model, the numerical singularities are avoided in the region where the tensor of strain rate equals 0 as long as $\theta\neq 0$. For the simulations discussed in the present work, the Princeton frictional model was selected since tests on two frictional models carried out by Breard et al. (2019) demonstrated that this model resulted in a more gradual variation of solid pressures into the granular material and in a better dissipation of the pore pressures than that obtained with the frictional model proposed by Schaeffer (1987). We remind the reader to the above-mentioned papers for a detailed description of P_{sm}^f.

The momentum transferred between the m^{th} and l^{th} solid phase (I_{ml} also referred to as solid-solid interaction force is represented by drag forces caused by velocity difference between the different solid phase and was modelled by Syamlal et al. (1987) using a simplified version of the kinetic theory:

$$I_{ml}=-\alpha_{sml}(U_{sl}-U_{sm}) \tag{7}$$

where α_{sml} is the drag coefficient, which is equal to:

$$\alpha_{sml}=\frac{3\left(1+e_p\right)\left(\pi/2+C_f\pi^2/8\right)\varepsilon_{sl}\rho_{sl}\varepsilon_{sm}\rho_{sm}(d_l+d_m)^2 g_{0lm}|U_{sl}-U_{sm}|}{2\pi\left(\rho_{sl}d_l^3+\rho_{sm}d_m^3\right)}+C_1P^* \tag{8}$$

where C_f is the friction coefficient between the solid phases, d is the particles diameter, g_0 is the radial distribution coefficient, C_1 is the segregation sloping coefficient (Gera et al., 2004) and P^* is represented by an empirical power law equals to $P^*=A(\varepsilon_g^*-\varepsilon_g)^{10}$, where A is equal to 1024 Pa. g_0 describes the probability of finding two particles at that specific location (Boyle and Massoudi, 1989), and it represents a correcting factor acting when concentration is quite high to break molecular chaos assumption (Dartevelle, 2004). The first term on the right-hand side of Eq. 8 accounts for the momentum transfer between

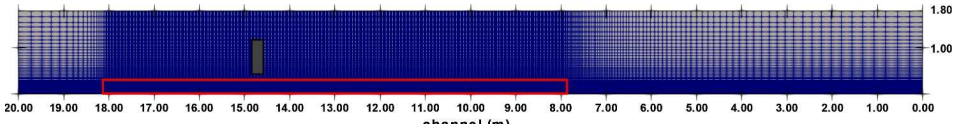

Fig. 1. Grid layout for the computational domain. The granular material is shaded grey, and the focus area is outlined by the solid red line.

the phases due to the collision and friction, while the second one is required to account for "hindrance" effects caused by enduring contacts between particles of different sizes and densities in real polydisperse granular mixtures (Gera et al., 2004). This happens when the particles are closely packed and the fines cannot percolate through the interstices of the packed bed, because of their size. However, in the TFM approach the solid phases are modelled as different interpenetrating continua, which will segregate by contrast of density even in packed bed. In order to take the "hindrance" effect into account avoiding the solid phases segregation in packed beds, Gera et al. (2004) proposed the simple expedient of increasing the upward solid-solid drag, forcing the different solid phases to move together and behave as a single phase. On basis of his work, Gera et al. (2004) suggest C_1 value of 0.3.

There are different radial distribution functions implemented in MFIX, which can be used either for polydisperse or monodisperse granular mixtures. In the present work, the radial distribution functions derived by Lebowitz (1964) and Mansoori et al. (1971) for polydisperse mixtures of hard-spheres and pure hard-spheres, respectively, were used. The Mansoori relation is written in MFIX as a Taylor series approximation (Van Wachem et al., 2001). Lebowitz and Mansoori models were modified by Iddir and Arastoopour (2005) and by Van Wachmen et al. (2001), respectively, to prevent non-converging iterations near maximum solid concentration. The used radial distribution functions are listed below:

$$g_{0lm} = \frac{1}{\varepsilon_g} + 3\frac{d_l d_m}{\varepsilon_g^2(d_l + d_m)}\sum_{\lambda=1}^{2}\frac{\varepsilon_\lambda}{d_\lambda} \quad \text{standard Lebowitz} \tag{9}$$

$$g_{0lm} = \frac{1-\varepsilon_g^*}{\varepsilon_g} + 3\frac{d_l d_m}{d_l + d_m}\sum_{\lambda=1}^{2}\frac{\varepsilon_\lambda}{d_\lambda} \quad \text{modified Lebowitz} \tag{10}$$

$$\varepsilon_{sml}^* = \begin{cases} \varepsilon_{sm}^* + \varepsilon_{sm}^*\left(1-\varepsilon_{sm}^*\right)\left(1 - 2.35\, r_{ml} + 1.35\, r_{ml}^2\right) & \text{if } r_{ml} \le 0.741 \\ \varepsilon_{sm}^* & \text{if } r_{ml} > 0.741 \end{cases} \tag{14}$$

$$g_{0lm} = \frac{1}{\varepsilon_g} + 3\frac{d_l d_m}{d_l + d_m}\frac{x_i}{\varepsilon_g^2} + 2\left(\frac{d_l d_m}{d_l + d_m}\right)^2\frac{x_i^2}{\varepsilon_g^3} \quad \text{standard Mansoori} \tag{11}$$

$$g_{0lm} = \frac{1-\varepsilon_g^*}{\varepsilon_g} + 3\frac{d_l d_m}{d_l + d_m}\frac{x_i}{(1-\varepsilon_g^*)^2} + 2\left(\frac{d_l d_m}{d_l + d_m}\right)^2 x_i^2\frac{(1-\varepsilon_g^*)^3}{\varepsilon_g} \quad \text{modified Mansoori} \tag{12}$$

where x_i is equal to $\sum_{i=1}^{m}(\varepsilon_{si}/d_i)$.

The transferred momentum between the gas and solid phase (I_{gm} also referred to as gas-solid interaction force is mainly due to drag forces exerted by the fluid on the solid phases and to buoyancy force generated by gas pressure gradient:

$$I_{gm} = -\varepsilon_{sm}\nabla P_g - \beta_{gm}\left(U_{sm} - U_g\right) \tag{13}$$

in which the first and the second term on the right-hand side indicate the buoyancy and the drag forces, respectively, while β_{gm} represents the solid-gas drag coefficient. Several researchers proposed different expressions to calculate the drag coefficient, among which Wen and Yu (1966), Gidaspow (1994), Syamlal and O'Brien (1988), Hill et al., (2001) and Benyahia et al. (2006). These relationships, which are listed in the summary of MFIX equations (https://mfix.netl.doe.gov/doc/mfix-archive/mfix_current_documentation/MFIXEquations2012-1.pdf; Benyahia et al., 2012), were selected for the sensitivity analysis reported in the Supplementary Material (Appendix). The drag coefficient is calculated for each solid phase considering it as a monodisperse system of equal overall void concentration. Hence, the calculation of the drag force exerted by the fluid on the mth solid phase does not consider the presence of the lth solid phase. Several authors proposed different expressions for the drag force experienced by a polydisperse particles system (Beetstra et al., 2007; Gidaspow, 1994; Patwardhan and Tien, 1985), and MFIX provides the possibility to use the relation proposed by Beetstra et al. (2007), which is based on the Carman-Kozeny approximation.

The maximum packing, which is fundamental for a correct calculation of the momentum exchange, is different for mono- and polydisperse systems in response to mixing of particles of different sizes. This leads to an increase of the maximum packing with increasing polydispersity because smaller particles fill initial voids of the coarser ones. To emulate this effect, two correlations to calculate the maximum packing of polydisperse mixtures are implemented in MFIX: Fedors and Landel (1979) and Yu and Standish (1987) correlations. The former is only suitable for bidisperse mixtures, while the latter is suitable for bi- and polydisperse systems. Both the correlations do not consider mixtures composed of irregular-shaped particles. In order to simulate granular flows without any limitation on the solid phases number, for the following simulations, the Yu and Standish relation was selected:

$$r_{ml} = \begin{cases} \dfrac{d_m}{d_l} & \text{if } m \ge l \\ \dfrac{d_l}{d_m} & \text{if } m < l \end{cases} \tag{15}$$

where ε_{sml} is the maximum packing of the mixture composed by the solid constituents mth and lth. The diameters are ordered from coarsest to finest particles ($d_1 \ge d_2 \ge d_3 \ge \ldots \ge d_n$) so that the solid phase m corresponds to the coarsest particle (d_1) and solid phase l change from the second to the last particle size (d_2, d_3,... d_n). Thus, the Yu and Standish relationship calculates the maximum packings for the different particles sizes couples (ε_{s12}^*, ε_{s13}^*, ...ε_{s1n}^*) and finally, the greatest ε_{sml}^* will be selected by MFIX code as the maximum solid concentration of the polydisperse granular mixture.

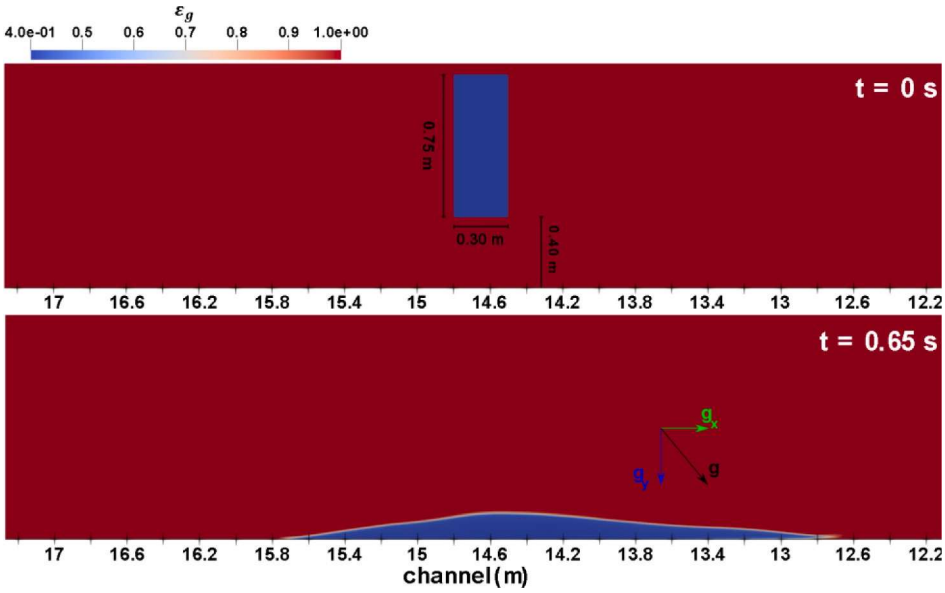

Fig. 2. Gas volume concentration (ε_g) at t = 0 s and t = 0.65 s. The green and blue arrows denote the gravitational accelerations in the x and y direction, while the black arrow indicates the resulting gravitational acceleration (from Neglia et al., 2022).

Table 2
Summary of solid and fluid phase parameters used in the simulations.

Parameters (unit)	Symbols	Bidisperse 1	Bidisperse 2
Solid density (kg/m^3)	ρ_s	2300	2300
Particles diameter (m)	d	$2 \cdot 10^{-3}$, $1 \cdot 10^{-3}$	$1 \cdot 10^{-3}$, $0.1 \cdot 10^{-3}$
Particle-particle restitution coefficient	e_p	0.9	0.9
Particle-wall restitution coefficient	e_w	0.7	0.7
Internal friction angle (°)	δ_{int}	35°	35°
Basal friction angle (°)	δ_w	13°	13°
Max packing fraction	ε_s^*	0.65	0.65
Solid concentrations	ε_s	0.25, 0.25	0.25, 0.25
Fluid density (kg/m^3)	ρ_g	1.2	1.2
Fluid dynamic viscosity (Pa s)	μ_g	$1.8 \cdot 10^{-5}$	$1.8 \cdot 10^{-5}$

3. The effect of the different drag formulations on bidisperse granular flow simulations

Sensitivity analysis of drag forces on g_0, e_p and β_{gm}were conducted in order to study the effect of changes in the drag force calculation on simulated bidisperse granular flows. Sensitivity analysis of the drag force exerted by the flow on the solid phases showed simulated granular flows almost insensitive to the variation of β_{gm}. This should not surprise because the granular flows under analysis are at high solids concentrations ($\varepsilon_s > 0.5$), in which case the gas-solid interaction play a negligible role. For this reason, the results of the sensitivity analysis on the fluid-solid drag force are reported in the Supplementary Material (Appendix). Instead, the results for the drag forces exerted by the lth on the mth solid phase (Eq. 7) are reported in the following Section. In the presented CFD simulations, the rectangular computational domain of 20.0 m length x 1.8 m height is discretized with a finer grid with rectangular

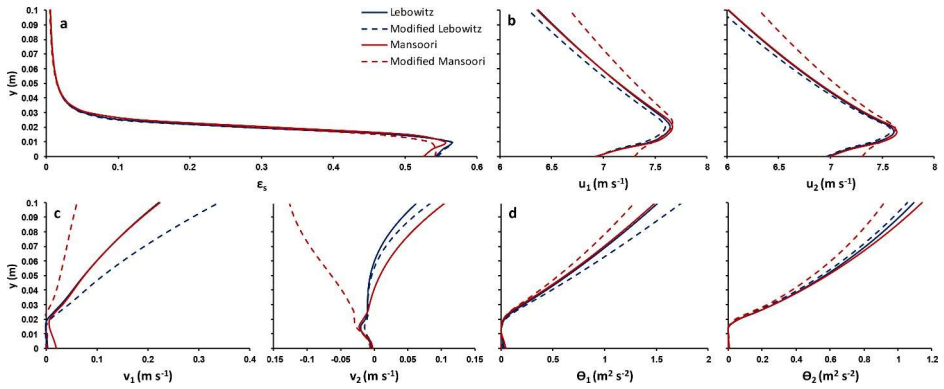

Fig. 3. Profiles of solid volume concentration (a), solid velocity in x (b) and y (c) direction and granular temperature (d) at 9 m from the right side of the domain (or 5.5 m downstream the initial position of the granular material) against the distance from the wall at changing g_0. The subscripts 1 and 2 refer to solid phases of 2 mm and 1 mm, respectively. t = 1.40 s.

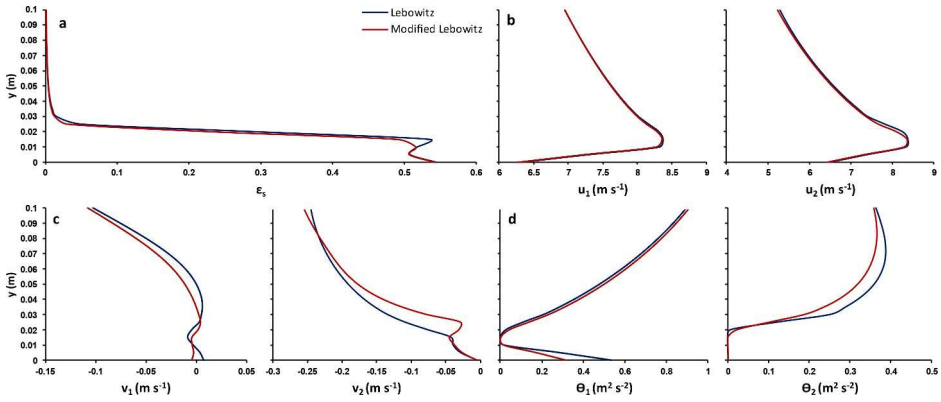

Fig. 4. Profiles of solid volume concentration (a), solid velocity in x (b) and y (c) direction and granular temperature (d) at 9 m from the right side of the domain (or 5.5 m downstream the initial position of the granular material) against the distance from the wall at changing g_0. The subscripts 1 and 2 refer to solid phases of 1 mm and 0.1 mm, respectively. t = 1.40 s.

cells of 0.02 m x 0.005 m in the focus area and with a coarser grid close to the boundaries (Fig. 1). All the simulations presented in the current work were ran using an adaptive time step and a second-order discretization scheme (Superbee) to solve the equations. The independence of the numerical solution from the choice of the grid size here presented is not reported in the current work because it was already demonstrated in Neglia et al. (2022) work.

The simulations were carried out by dropping granular material from a height of 0.40 m on a 40° inclined channel, which was reproduced through tilting the component of gravitational acceleration at the instant when the center of gravity of the granular mixture impacts onto the channel surface (Fig. 2).

The particles diameters of the simulated mixtures were set to 1 mm – 0.1 mm and to 2 mm – 1 mm. The simulations were performed by using for solid and gas phases partial-slip and no-slip boundary conditions, respectively. The used partial-slip wall condition was that proposed by Jenkins (1992). The reader is referred to Neglia et al. (2022) for a detailed analysis of the partial-slip wall conditions for the solid phases implemented in MFIX. The solid and fluid phase physical parameters are listed in Table 2.

3.1. Sensitivity analysis of drag forces experienced between solid phases on radial distribution function and restitution coefficient

The drag force experienced between two solid phases is calculated by means of Eq. 7, which is regulated by the drag constant α_{sml} that depends on iteratively calculated flow parameters (ε_s, g_0, U_s) and on constant granular flow parameters (e_p, d, ρ_s, C_f, C_1) Eq. 8). For the following sensitivity analysis, the effect of the radial distribution function g_0 and the particle-particle restitution coefficient e_p on the drag force calculation and consequently, on the simulated bidisperse granular flows was studied. As above-mentioned, g_0 differs for mono- and polydisperse particles systems and for this study, the Lebowitz and Mansoori models (Eqs. 9 – (12) were selected. The segregation slope coefficient C_1 (Gera et al., 2004) was not considered because the simulated granular mixtures were composed by solid phases with identical densities.

For changing g_0 and for bidisperse granular flows of 2 mm – 1 mm and 1 mm – 0.1 mm, profiles of solid volume concentration (ε_s), solid velocity in x and y direction (u_s and v_s) and granular temperature (θ), at a simulation time (t) of 1.40 s, are reported in Figs. 3 and 4, respectively.

The vertical profiles of ε_s (Fig. 3a) show almost identical flow thickness, with very slight variations in the maximum solid concentrations, which range between values of 0.5 – 0.6, and in the maximum u_s for the two solid phases, which reach maximum values of ca. 7.6 m s^{-1} (Fig. 3b). On the other hand, v_s profiles show different behaviour at changing g_0 (Fig. 3c). The standard and modified Lebowitz profiles exhibit positive values (upward particles movement) for the top 80% of the flow height for both the solid phases, whereas for the 20% close the flow base the coarse and fine particles record different regimes. In particular, the solid phases 1 and 2 (d_1 = 2 mm, d_2 = 1 mm) show neutral values (close to v_s = 0 m s^{-1}) and a small negative peak (downward particles movement), respectively. Negative vertical velocities indicate solid phase fall driven by gravity and by solid volume concentration; positive vertical velocities indicate solid phase moving upward into upper layers. On the other hand, the standard Mansoori trend follows the previous ones, while the modified Mansoori profile for

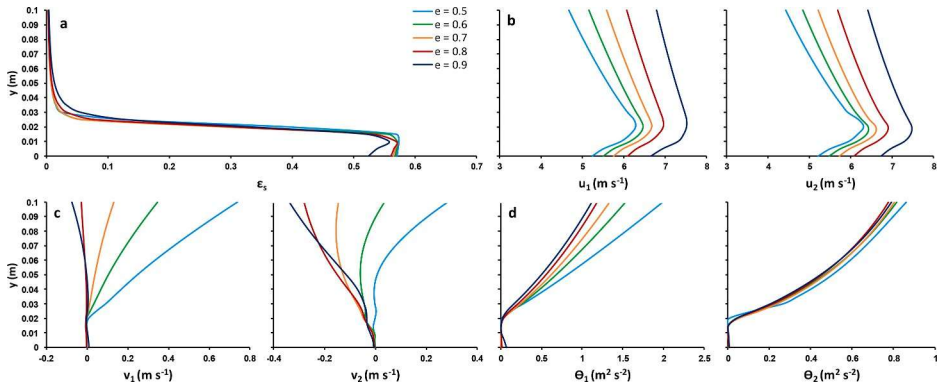

Fig. 5. Profiles of solid volume concentration (a), solid velocity in x (b) and y (c) direction and granular temperature (d) at 9 m from the right side of the domain (or 5.5 m downstream the initial position of the granular material) against the distance from the wall at changing e_p. The subscripts 1 and 2 refer to solid phases of 2 mm and 1 mm, respectively. t = 1.55 s.

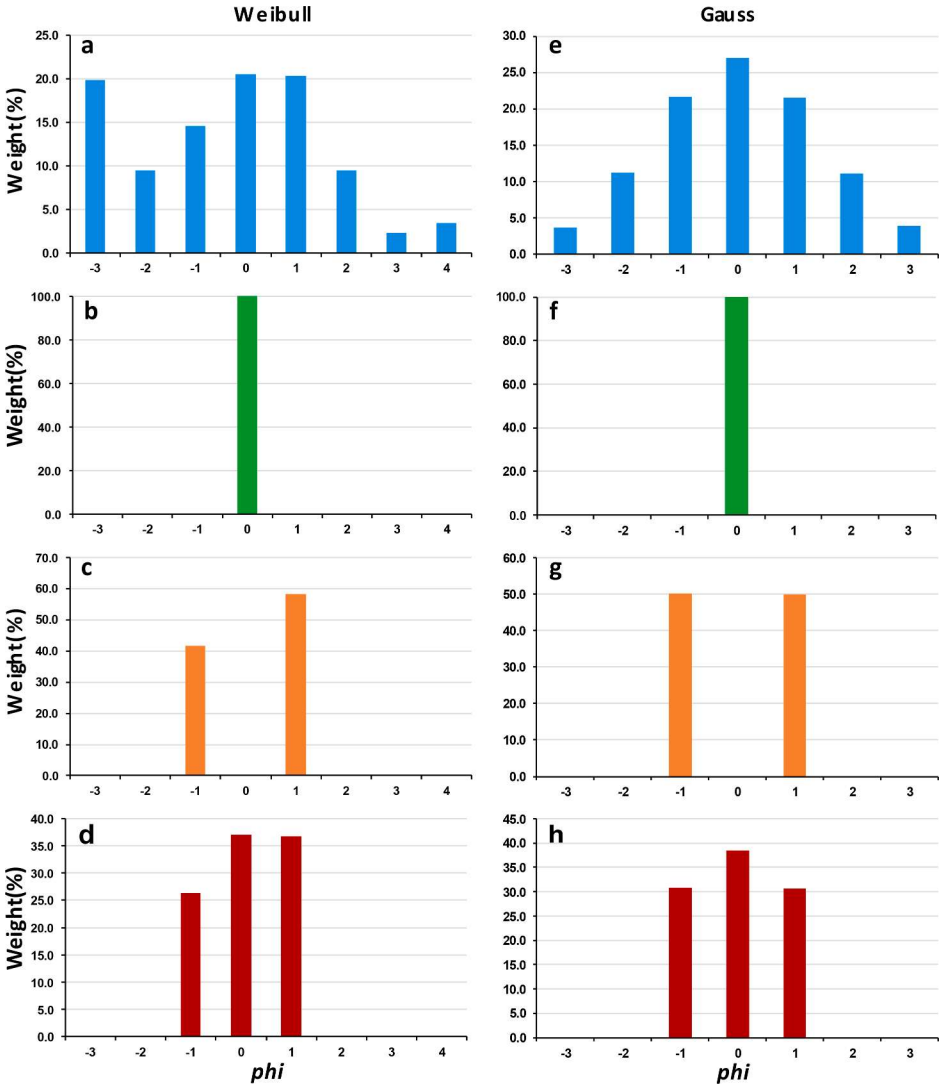

Fig. 6. Grain size histograms of a, e) the experimental modified Weibull and Gaussian granulometric distributions, and of the b, f) mono-, c, g) bi- and d, h) tri-disperse granulometric distribution used for the simulations. $phi = -\log_2 d$.

d_2 diverges from the other ones exhibiting negative values for the whole flow thickness (Fig. 3c). It is worth noting that the coarsest solid phase tends to migrate upward whereas the finest one tends to be segregated in the basal layer. Finally, all θ profiles record the highest values in the portion of the flow where ε_s is at its minimum (Fig. 3d) and then θ decreases approaching the channel surface where ε_s increases. Greater ε_s results in lower θ because the particle fluctuations are inhibited or almost suppressed in the most concentrated layer of the flow where ε_s is maximum, and enhanced in the top flow that is more diluted. Furthermore, high ε_s promote the granular temperature dissipation as heat during the inelastic collisions.

The simulations' results for the bidisperse granular flow of 1 mm – 0.1 mm (Fig. 4) do not report the profiles for the Mansoori models, because they showed numerical solution divergence when the granular mixture impacts the channel surface, i.e. during the material compaction phase. ε_s, u_s and v_s profiles show almost equal flow thicknesses and velocities for both the radial distribution functions (Fig. 4a, b and c). u_s reaches maximum values that range from 8.0 m s^{-1} to 8.5 m s^{-1}, which are 0.5 m s^{-1} higher than velocities developed by the bidisperse mixture of 2 mm – 1 mm (Fig. 3b). v_s profiles generally show negative velocities in the entire flow thickness, with small positive or neutral values close to the channel surface for the coarse solid phase ($d_1 = 1$ mm). θ profiles for the solid phase 1 record high θ of ca. 0.3 m^2 s^{-2} – 0.5 m^2 s^{-2} close to the channel surface that decrease in the flow center and again increase to the top of the flow, whereas the solid phase 2 shows θ close to 0 m^2 s^{-2} for the 20 % near the flow base that upward increase (Fig. 4d).

The flow parameters profiles at changing e_p for bidisperse granular flows of 2 mm – 1 mm, at a simulation time of 1.55 s, are reported in Fig. 5. The simulated bidisperse granular mixture of 1 mm – 0.1 mm developed numerical instabilities and numerical solution divergence during the critical compaction phase for each e_p lower than 0.9 ($e_p < 0.9$). For this reason, the results for bidisperse granular flow of 2 mm – 1 mm are only reported (Fig. 5). Solution divergence, observed during the compaction phase for the sensitivity analysis on the restitution coefficient and the radial distribution function, could be due to exceeding the maximum packing enabled in MFIX. The high mobility of the finer solid phase enhanced by kinetic energy acquired from the material dropping could be the reason of this instability condition.

ε_s vertical profiles show almost identical flow thickness of ca. 0.03 m, with maximum solid concentration of ca. 0.55 (Fig. 5a), while u_s profiles exhibit velocities increase for higher restitution coefficients. The velocity increase at increasing e_p should not surprise because the restitution coefficient measures the recovery of kinetic energy after the collision and can be obtained from the ratio of the velocity of the particles after and before the collision. Hence, the greater e_p, the lower the dissipation rate given by inelastic collisions, which results in lower

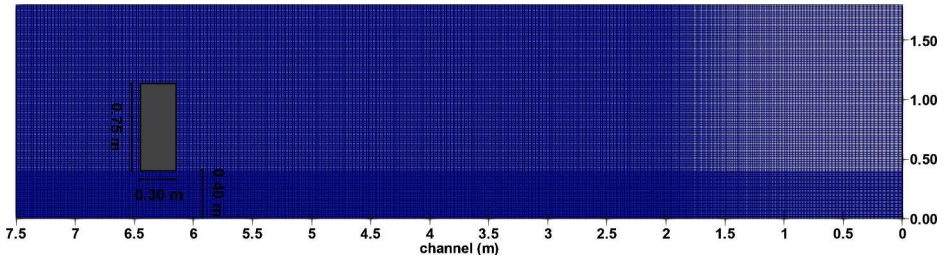

Fig. 7. Grid configuration for the computational domain. The granular material is shaded grey.

Table 3
Summary of solid and fluid phase parameters used in the simulations.

Parameters (unit)	Symbols	1° experiment	2° experiment (Gaussian)	3° experiment (Weibull)
Solid density (kg/m^3)	ρ_s	2300	2300	2300
Monodisperse particles size (m)	d	$1 \cdot 10^{-3}$	$1 \cdot 10^{-3}$	$1 \cdot 10^{-3}$
Bidisperse particles size (m)	d	$2 \cdot 10^{-3}$, $1 \cdot 10^{-3}$	$2 \cdot 10^{-3}$, $0.5 \cdot 10^{-3}$	$2 \cdot 10^{-3}$, $0.5 \cdot 10^{-3}$
Tridisperse particles size (m)	d	$2 \cdot 10^{-3}$, $1.5 \cdot 10^{-3}$, $1 \cdot 10^{-3}$	$2 \cdot 10^{-3}$, $1 \cdot 10^{-3}$, $0.5 \cdot 10^{-3}$	$2 \cdot 10^{-3}$, $1 \cdot 10^{-3}$, $0.5 \cdot 10^{-3}$
Particle-particle restitution coefficient	e_p	0.9	0.9	0.9
Particle-wall restitution coefficient	e_w	0.7	0.7	0.7
Internal friction angle (°)	δ_{int}	33°	30°	30°
Basal friction angle (°)	δ_w	13°	13°	13°
Max packing fraction	ε_s^*	0.65	0.65	0.65
Monodisperse solid concentration	ε_s	0.5	0.5	0.5
Bidisperse solid concentrations	ε_s	0.25, 0.25	0.26, 0.24	0.21, 0.29
Tridisperse solid concentrations	ε_s	0.15, 0.20, 0.15	0.15, 0.20, 0.15	0.13, 0.19, 0.18
Fluid density (kg/m^3)	ρ_g	1.2	1.2	1.2
Fluid dynamic viscosity (Pa s)	μ_g	$1.8 \cdot 10^{-5}$	$1.8 \cdot 10^{-5}$	$1.8 \cdot 10^{-5}$
Specularity coefficient	ϕ	0.1	0.1	0.1

momentum dissipation and higher flow velocities (Fig. 5b). v_s profiles show gradual changes at increasing restitution coefficient, with positive velocities that pass into negative values (Fig. 5c). The positive-negative transition is recorded at different e_p values for the two solid phases indeed, the coarse solid phase ($d_1 = 2$ mm) captures the passage from positive to negative velocities for e_p greater than 0.7, whereas the fine solid phase ($d_2 = 1$ mm) shows this transition for e_p greater than 0.5. As regards the granular temperatures, all the profiles record values close to 0 m^2 s^{-2} for the flow where ε_s reaches its maximum, after increasing to the top of the flow (Fig. 5d).

4. Increasing the model complexity: from mono- to tridisperse granular flows

In order to conduct a sensitivity analysis of the flow variables on the number of solid phases and in order to observe the polydispersity effects on the granular flow front velocities, three large-scale experiments produced at the Mexican large-scale flume facility (LAIMA laboratory, Geology Institute of the University of San Luis Potosì, Mexico) were simulated, approximating the experimental granular material with mono-, bi- and tridisperse granular mixtures. Other solid phases were not added because of the required considerable computational power. The flume facility was composed by a hopper with a remotely controlled opening located 0.40 m above the inlet of a 5-2 long and 0.30 m wide channel with an inclination of 40°. Specific details on the instrumental apparatus and the experiments are available in (Rodriguez-Sedano et al., 2016; Sulpizio et al., 2016). The granular material of the first experiment is the same used for the benchmark analysis of Neglia et al. (2022), in which the particles diameters ranged between 1 mm and 2 mm; the second and the third ones correspond to two of the experiments reported in the work of Sulpizio et al (2016), where the experimental material had a modified Weibull-type, to which was added a coarse-grained material of 8 mm, and a Gaussian-type granulometric distributions, respectively (Fig. 6a and e). The volcanic material used in the above-mentioned experiments was composed by samples of poorly vesicular dacitic clasts ($\rho_s \cong 2300$ kg/m^3) with a weight of ca. 41 kg. The first experiment was approximated by mono- (1 mm), bi- (1 mm and 2 mm) and tridisperse (1 mm, 1.5 mm and 2 mm) granular mixtures, while the solid phases sizes of granular flows used to simulate the second (Weibull) and the third (Gaussian) experiments were set to 1 mm, 2 mm – 0.5 mm and 2 mm – 1 mm – 0.5 mm, considering the particles sizes range with the greater percentage by weight (Fig. 6). Bidisperse flows of 2 mm – 0.5 mm were selected for the Weibull and Gaussian cases to emphasize the polydispersity effect on the flow. It is worth noting that the greatest particles size ($phi = -\log_2 d = -3$) for the Weibull case (Fig. 6a), which would be the third granulometric class in terms of percentage by weight, was not considered because it would require very large computational cells (ca. 8 cm) in order to maintain the TFM assumption on the size of the CV that has to be at least ten times greater to the particles one.

The rectangular computational grid of 7.5 m x 1.8 m is made of a finer grid with square cells of 0.01 m side in the compacting and sliding zone and of a coarser one to the top and to the right of the domain (Fig. 7).

Because the action of the fluid on the coarser solid phases has proven to be poorly influent on the flow parameters, the MFIX default drag force relationship, i.e. the Syamlal and O'Brien (1988) one, was selected for the calculation of the drag coefficient β_{gm}. The standard and modified Lebowitz relationships (Eqs. 9 and 10, respectively) resulted in very similar flow variables profiles, avoiding problems of numerical solution divergence during the material compaction phase (Fig. 4). For the above-mentioned reasons, the Lebowitz expression was selected to calculate g_0 for polydisperse systems. The fluid and solid phase parameters are listed in Table 3.

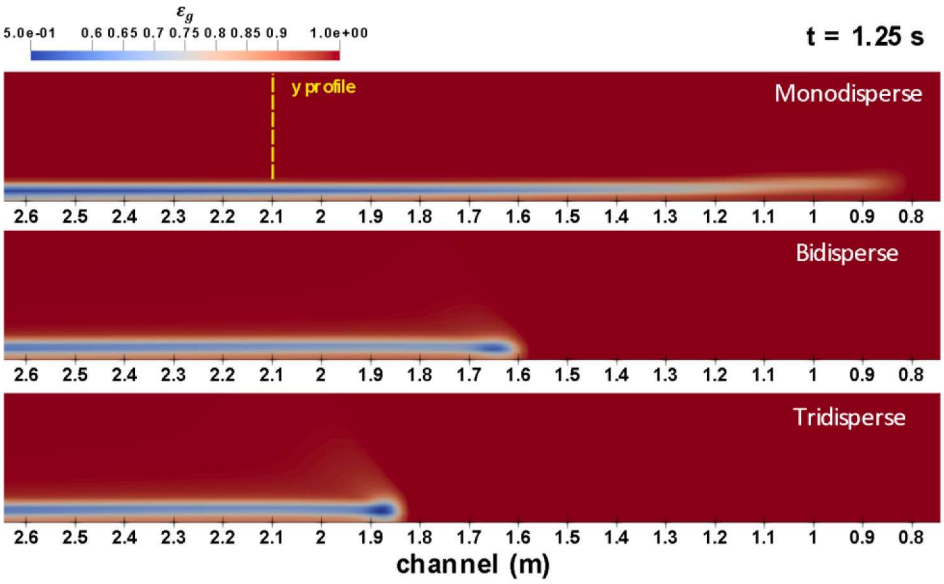

Fig. 8. Plots of gas volume concentration (ε_g) of the mono-, bi- and tridisperse granular flows. The yellow dotted line marks the profiles position shown below. t = simulation time.

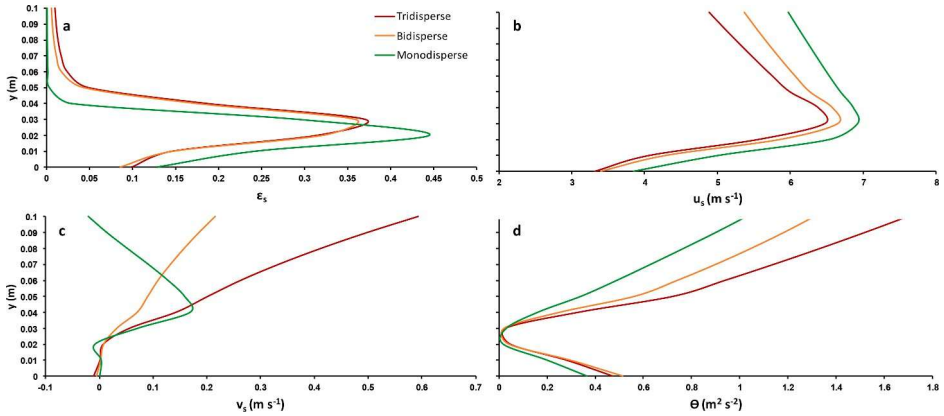

Fig. 9. Mono-, bi- and tridisperse granular mixtures profiles of solid volume concentration (a), solid velocity in x (b) and y (c) direction and granular temperature (d) at 4.35 m of the sloped channel against the distance from the wall. u_s, v_s and θ of polydisperse granular flows are referred to solid phase of 1 mm, while the coarser solid phases are not reported. t = 1.25 s.

4.1. Sensitivity analysis of the flow parameters to the number of solid phases

Simulations at increasing number of solid phases were carried out in order to analyse the effect of polydispersity on the flow variables and on the diluted layer that forms at the base of the simulated granular flows, when the Johnson and Jackson boundary condition is selected. This diluted layer was referred by Neglia and Co-Workers (2022) as "air--cushion" and a very similar phenomenon was shown by Lube et al. (2019) by coupling numerical multiphase modelling (MFIX-DEM) and large-scale experiments on dilute pyroclastic flows. After a preliminary benchmark study of the boundary conditions implemented in MFIX against one experimental granular flow, the same authors showed how the simulations with the Johnson and Jackson boundary condition and with a specularity coefficient (ϕ) of 0.1 resulted in the best match with the experimental data. ϕ depends on the particle and wall properties, including the surface roughness, and varies between zero for perfectly specular collision and unity for perfectly diffuse collisions (Johnsons and Jackson, 1987). For the reason explained before, we used the same boundary condition for this analysis. We only reported the results of the simulations on the first experiment because they are very similar to those ones obtained from the simulations on the other two test cases. Plots and profiles of solid volume concentration, solid velocity in x and y direction and granular temperature are reported in Figs. 8 and 9.

Mono-, bi- and tridisperse particles systems show different flow front shape (Fig. 8). The monodisperse mixture has a dispersed flow front with a well-developed diluted layer at the base, while the bi- and tridisperse fronts develop elliptical and spherical shape, respectively (Fig. 8). The greatest ε_s of polydisperse mixtures are associated to the granular flow fronts (Fig. 8). Vertical profiles of the solid volume concentration detect diluted layer at the flow base for mono- and poly-disperse granular flows (Fig. 9a). The slight difference in the thickness of this layer between mono- and polydisperse mixtures is given by the different position of the granular flow front regarding the profile position (yellow dotted line in Fig. 8). In fact, ε_s plots clearly show that the monodisperse granular flow is faster than the polydisperse ones (Fig. 8). This is also observed from the profiles of solid velocities in the x-direction (u_s), which exhibit greater maximum velocities by decreasing the solid phases number (Fig. 9b). v_s profiles show different behaviours between mono- and poly-disperse granular mixtures (Fig. 9c): the bi- and tridisperse granular flows have almost neutral velocities close to the channel surface that pass into positive values in the upper flow, while the monodisperse one

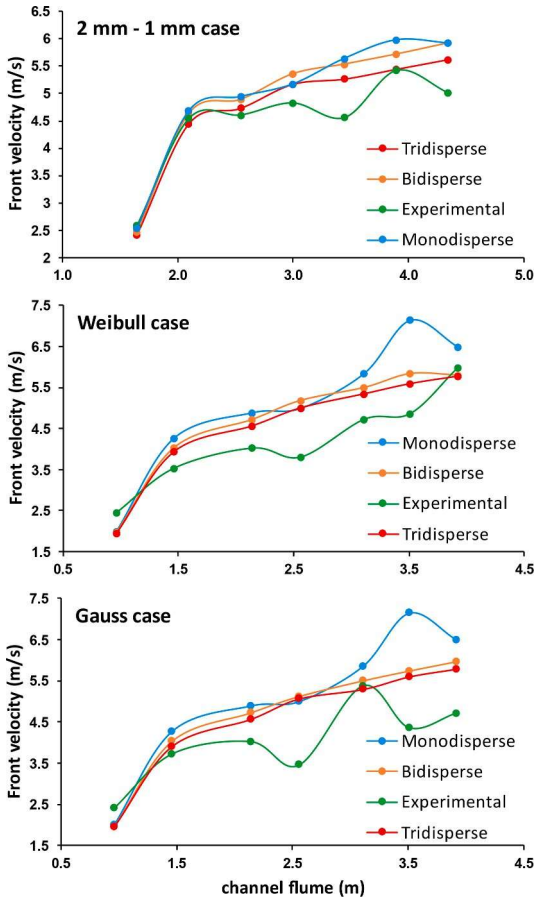

Fig. 10. Simulated and experimental granular flow front velocities of the three experimental cases plotted against the channel flume. Dots indicate laser detectors (L) position along the channel.

yields a complex velocity trend, showing neutral and small negative values in the basal layer that pass into positive values in the flow centre and slightly negative to the top of the flow (Fig. 9c). In particular, the positive v_s recorded by the tridisperse system are ca. 0.40 m s^{-1} – 0.60 m s^{-1} greater than mono- and bidisperse case. Finally, the solid phases number also influences θ profiles showing the highest values of 1.70 m^2 s^{-2} for the tridisperse flow (Fig. 9d). All profiles exhibit values close to 0 m^2 s^{-2} at maximum ε_s (Fig. 9a) that increase in the upper and lower part of the granular flow. The high granular temperatures in the basal layer are allowed by the air-cushion presence.

4.2. Polydispersity effects on the granular flow front velocity

The polydispersity effect on the front propagation velocity was studied comparing mono-, bi- and tridisperse granular flow front velocities with the experimental ones obtained by seven laser detectors along the inclined channel flume used to produce the three large-scale experiments (Sulpizio et al. 2016). The velocity profiles are reported in Fig. 10.

Considering the 2 mm- 1 mm case, the initial experimental rapid increase of velocity followed by an oscillatory trend around ca. 4.0 m s^{-1} with a final larger velocity peak of 5.4 m s^{-1} is well replicated by the simulated granular flows (Fig. 10). The monodisperse granular flow also mimic the final velocity oscillation of 6.1 m s^{-1} in proximity of the laser detector L6, reaching the final velocity value of 5.9 m s^{-1} at L7. On the contrary, the simulated bi- and tridisperse granular flows do not capture this experimental feature, resulting in an approximately linear increase in velocity from positions L5 to L7 reaching maximum velocities of 5.8 m s^{-1} and 5.6 m s^{-1}, respectively. Deviation of the simulated data from the experimental ones was calculated by means of the mean square error equals to 0.36 m^2 s^{-2}, 0.32 m^2 s^{-2} and 0.15 m^2 s^{-2} for mono-, bi- and tridisperse granular flows, respectively.

In the Weibull and the Gaussian cases, the granular flows record gradual velocities increase overlaid by velocity oscillations, reaching the maximum values of 5.9 m s^{-1} and 5.4 m s^{-1}, at the laser detectors L7 and L5, respectively (Fig. 10). The monodisperse granular flows, which are equal for both the cases, replicate quite well the experimental velocity trend and generate flow front velocities generally greater than experimental ones. The great final velocity peaks of 7.1 m s^{-1} recorded by the monodisperse flow in proximity of L6 is not detected for the experimental Weibull case, while it is recorded ahead, at the fifth laser detector, for the experimental Gaussian case. As seen for the first experiment, the simulated polydisperse granular flows show very low amplitude oscillations and magnitude velocities closer to the real ones. Mono-, bi- and tridisperse granular mixtures used to replicate the Weibull and the Gaussian cases produce maximum flow front velocities of 7.1 m s^{-1}, 5.8 m s^{-1} and 5.7 m s^{-1} and of 7.1 m s^{-1}, 6.0 m s^{-1} and 5.8 m s^{-1}, respectively, and mean square errors thereon of 1.37 m^2 s^{-2}, 0.64 m^2 s^{-2} and 0.44 m^2 s^{-2} and of 2.11 m^2 s^{-2}, 1.01 m^2 s^{-2} and 0.83 m^2 s$^{-2,}$ respectively (Fig. 10). The latter are higher than errors obtained for the Weibull case.

5. Final discussions

In polydisperse multiphase mixtures, the drag forces between the individual solid phases are required to the momentum conservation equations for the solid phases Eqs. 4 and (5). This drag force modelled by means of the drag constant α_{sml}, which depends on constant and on iteratively calculated flow parameters (Eq. 8). For this study, we selected two parameters in order to study their effect on the drag force calculation and consequently, on the simulated motion of bidisperse granular flows: i) the radial distribution function g_0 and ii) the particle-particle restitution coefficient e_p. The sensitivity analysis was carried out using two different bidisperse granular mixtures composed by particles diameters of 2 mm and 1 mm and of 1 mm and 0.1 mm, respectively.

The sensitivity analysis of bidisperse granular flow of 2 mm – 1 mm on g_0 showed v_s profiles with different behaviour for fine and coarse particles. Indeed, the coarser ones recorded particles overpassing into the upper layer, whereas the finer solid phase captured a flow dominated in the basal part by particles fallout (Fig. 3c). The different behaviour of fine and coarse particles emulates segregation phenomena as kinetic sieving and kinematic squeezing active in real granular flows, which promote the downward migration of smaller particles through inter-granular voids of the larger ones and induce the apparent upward migration of the coarser particles, respectively (Sulpizio et al., 2014). The segregation of the finer solid phases increases the solid volume concentration at the flow base, which can raise up to the maximum packing calculated by means of the Yu and Standish (1987) correlation. Thus, a simulated bidisperse granular flow, which is able to replicate segregation dynamics, better approach the behaviour of the real granular flows than the simplest monodisperse systems. Finally, the modified Masoori model diverges from the others radial distribution functions showing a flow completely dominated by downward particles movement. This evidence, coupled with absence of detailed benchmark of g_0 against large-scale experiments on polydisperse mixtures, suggests the usage of Lebowitz and standard Mansoori relationships to simulate bidisperse granular flows.

The sensitivity analysis of bidisperse granular flows of 2 mm – 1 mm to e_p showed the increase of the flow front velocity with increasing the restitution coefficient (Fig. 5b). As mentioned above, the restitution coefficient is related to the amount of the original kinetic energy that is restored to the particles after collision. Hence, the greater e_p, the lower the dissipation rate of the inelastic collisions and, consequently, the faster simulated granular flows. The effect is significant even in flows

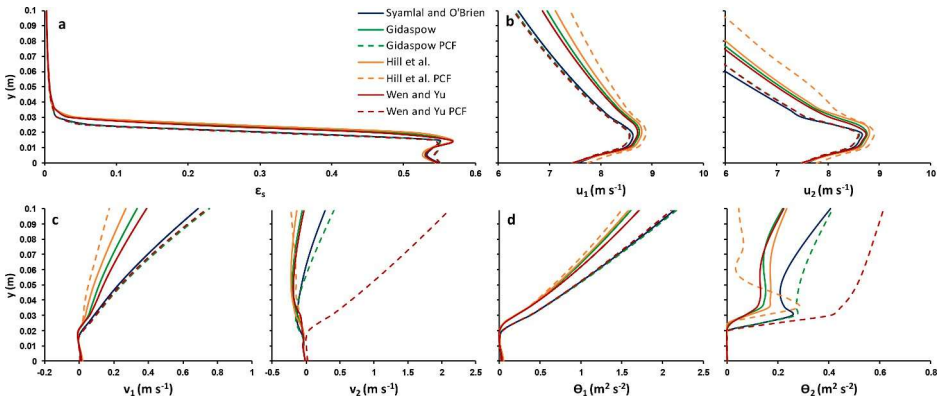

Fig. 11. Profiles of solid volume concentration (a), solid velocity in x (b) and y (c) direction and granular temperature (d) at 9 m from the right side of the domain (or 5.5 m downstream the initial position of the granular material) against the distance from the wall at changing β_{gm}. The subscripts 1 and 2 refer to solid phases of 1 mm and 0.1 mm, respectively. PCF states for "polydisperse correction factor". t = 1.20 s.

like those presented in this work, in which the particle concentration is close to the maximum packing, the granular temperature (a proxy of the collisions rate) is low almost everywhere in the flow (e.g., Fig. 3), hence the contacts between particles are primarily frictional. The seemingly contradictory sensitivity of the flow velocity on e_p is justified by the presence of the restitution coefficient in the drag constant (α_{sml}) calculation (Eq. 8), in which it acts as multiplier of the velocity difference between two solid phases ($|U_{sl} - U_{sm}|$). The significance effect of e_p also in flows dominated by frictional processes justifies the effort to obtain realistic estimates of e_p, which is not trivial. Even if the measurement of e_p for two spherical particles is relatively simple because it requires the measurement of the particles velocities after and before the collision, the restitution coefficient calculation for irregularly shaped polydisperse particles (as is the case of volcanic particles) becomes very challenging and remains an unsolved problem. For CFD simulations of complex particles systems, and in the absence of directly measured e_p, this parameter is derived from comparison between experimental and numerical data (Li and Benyahia, 2012; Louge et al., 1991). Unfortunately, the number of granular flows in the experimental campaign we refer to in this work is still no enough to obtain a reasonable value of e_p, and consequently we used e_p as a starting reference value of 0.9 in agreement with previous analogous works(Breard et al., 2019; Dartevelle, 2004; Gera et al., 2004; Li and Benyahia, 2012; Louge et al., 1991; Srivastava and Sundaresan, 2003), but we remain aware of the fact that e_p should be analyzed in detail by means of ad hoc studies.

The sensitivity analysis on the solid phases number emphasized the polydispersity effect on the flow propagation (Figs. 8 and 9). Indeed, by increasing the number of the solid phases, the flow front velocity decreased (Fig. 8). On the contrary, v_s and θ values increased for greater solid phases number (Fig. 9c and d). Hence, if on one hand the polydisperse granular flows developed lower velocities along the channel flume direction (u_s), on the other hand they resulted in greater velocity in the vertical direction (v_s), which enhances the segregation dynamics. u_s and v_s variations and the different flow fronts shape can be explained considering the solid-solid and gas-solid interaction forces I_{ml} and I_{gm}, which on basis of their sign exert on the solid phases downward/leftward (-) or upward/rightward (+) forces. Both the interaction forces depend on the solid phase concentration, which in the simulated polydisperse systems is calculated by means of Yu and Standish (1987) correlation (Eq. 14) that, by emulating the void filling by the smaller particles, results in greater ε_s. Consequently, the greater solid concentrations of the polydisperse mixtures, affecting I_{ml} and I_{gm}, play an important role in mixing and segregation processes of polydisperse system, resulting in granular flow front with higher ε_s and more defined shapes than monodisperse simulation (Fig. 8).

Generally, the polydisperse granular flows showed linear velocity increase from L2 to L7 with oscillations smoother than those ones recorded by monodisperse granular flows, which better mimic the experimental oscillatory trend. Nonetheless, the bi- and tridisperse simulations developed front velocities closer to the experimental ones (Fig. 10). The greater error decrease for the second and the third experiments is due to the higher heterogeneity of the used experimental material that was composed by seven or eight grains sizes (Fig. 6) against the single grain size of 0 *phi* (1 mm < d < 2 mm) that composed the granular material of the first experiment. Hence, three solid phases significantly increase the accuracy of the simulated data and probably a further increase in the number of simulated solid phases number would further improve the accuracy of the simulation, especially in the case of the second experiment. These findings suggest that polydispersity effect on the simulated granular flow front velocity is tangible and should not be neglected in simulations setting of experimental and natural polydisperse mixtures.

6. Conclusions and future perspectives

This work collects insights of polydispersity effect on the momentum calculation of gas and solid phases and hence, on the simulated polydisperse flow behaviour. Critical factors to consider to simulate polydisperse particles systems were highlighted, mixing and segregation phenomenon induced by non-uniformity of solid phases size were recorded and analysed and important findings on the granular flow velocities were carried out. Indeed, the polydisperse granular flows proved that the greater the number of the solid components, the lower the flow velocity. This evidence suggests that a best match between simulated and real flow velocities could occur researching feasible and simple methods, in terms of computational cost, to adequately represent the polydispersity of real granular flows in CFD simulations. However, many comparisons between simulated and experimental granular mixtures are still required to definitively understand if mono- and bidisperse particles systems, usually used to approximate real granular flows (e.g. Dartevelle et al., 2004; Sweeney and Valentine, 2017; Valentine and Sweeney, 2018; Breard et al., 2019; Valentine, 2020), are able to capture fundamental physics of polydisperse granular flows, as the volcanic ones, characterized by intrinsic complexity of the solid phase, which is represented by volcanic sediments that usually show a wide range of sizes, densities and shapes. Furthermore, the complexity of the volcanic particles systems is associated to the need to find experimental solutions to satisfactorily and accurately calculate the restitution coefficient, which impacts on the dissipation rate of the inelastic particle-particle collisions, and thus on the velocity of the simulated granular flows.

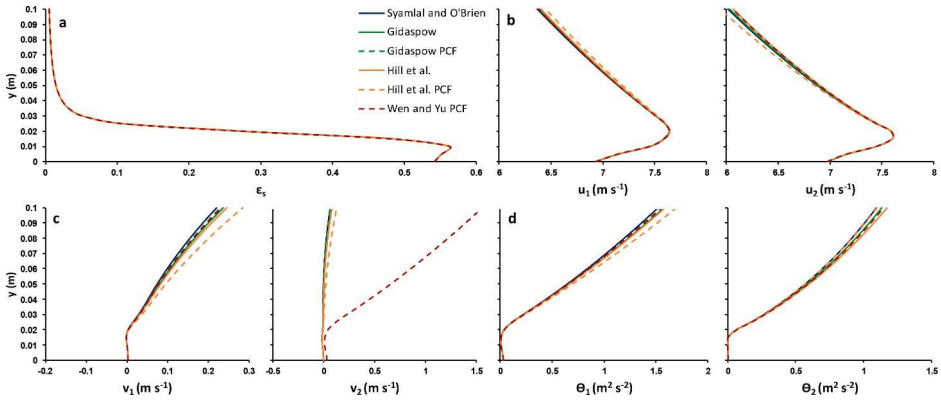

Fig. 12. Profiles of solid volume concentration (a), solid velocity in x (b) and y (c) direction and granular temperature (d) at 9 m from the right side of the domain (or 5.5 m downstream the initial position of the granular material) against the distance from the wall at changing β_{gm}. The subscripts 1 and 2 refer to solid phases of 2 mm and 1 mm, respectively. PCF states for "polydisperse correction factor". t = 1.28 s.

CRediT authorship contribution statement

Francesco Neglia: Conceptualization, Methodology, Software, Investigation, Writing – original draft. **Roberto Sulpizio:** Conceptualization, Writing – review & editing. **Fabio Dioguardi:** Conceptualization, Methodology, Software, Writing – review & editing. **Damiano Sarocchi:** Resources, Writing – review & editing.

Declaration of Competing Interest

The authors declare that they have no known competing financial interests or personal relationships that could have appeared to influence the work reported in this paper.

Data Availability

Data will be made available on request.

Appendix: sensitivity analysis of drag force exerted by the flow on solid phases

The drag force exerted by the flow on the solid phases depends on the drag coefficient β_{gm} (Eq. 13), which can be calculated by different relationships. The expressions tested with MFIX were those proposed by Wen and Yu (1966), Syamlal and O'Brien (1988), Gidaspow (1994) and Hill et al. (2001). All these models, except the Syamlal and O'Brien relationship, are implemented in MFIX with the polydisperse correction factor introduced by Beetstra et al. (2007). Sensitivity analysis on the listed relationships were carried out to study their incidence on the simulated bidisperse granular flow behaviour. The drag relationships with the polydisperse correction factor will be indicated in the following by the acronym "PCF".

Profiles of solid volume concentration (ε_s), solid velocity in x and y direction (u_s and v_s) and granular temperature (θ) at changing β_{gm} for bidisperse granular flows of 1 mm – 0.1 mm and 2 mm – 1 mm, at a simulation time of 1.20 s, are reported in Figs. 11 and 12, respectively.

The simulated bidisperse granular mixtures proved to be less sensitive to the variations of the drag force exerted by the flow on the solid phases with regard of the drag force between two solid phases. As mentioned in Section 3, in dense granular flows, the gas-solids interaction play a negligible role. Nonetheless, the simulated flow regimes in the uppermost parts of the flow were sensitive to the relationships to calculate the drag coefficient β_{gm}, showing important changes in the vertical velocity profiles (Fig. 11c), with particular emphasis on the fine solid phase of the bidisperse granular flow of 1 mm – 0.1 mm. More precisely, for the fine solid phase (d_2 = 0.1 mm), Hill et al. (2001), Hill et al. PCF, Gidaspow (1994) and Wen and Yu (1966) relationships resulted in flows dominated by particles fall; Syamlal and O'Brien (1988) and Gidaspow PCF resulted in two-piece flows, where the upper and the basal flow were dominated by upward particles movement and by particles fall, respectively; Wen and Yu PCF generated a flow dominated by the downward particles movement (Fig. 11c). On contrary, the coarse solid phase (d_1 = 1 mm) recorded upward particles movements for every drag relationship (Fig. 11c). The sensitivity analysis of this bidisperse granular mixture leads to three main conclusions: 1) the same drag model, whether or not the polydisperse correction factor, resulted in different flow regimes in the uppermost parts of the flow with particular emphasis on Wen and Yu (1966) and Wen and Yu PCF relationships, which developed opposite flow regimes demonstrating PCF impact on the simulated bidisperse granular flows; 2) the fine and coarse solid phases tend to move downward and upward, respectively, inside the simulated flow, triggering segregation phenomenon; 3) the downward movement of fine solid phases has important consequence on the velocity of the simulated flow indeed, the bidisperse granular flow of 2 mm – 1 mm records maximum velocities of 1.0 m s^{-1} lower than those ones recorded by bidisperse granular flow of 1 mm – 0.1 mm (Figs. 11b and 12b), highlighting the role of the fine solid phases on the flow mobility. To quantitatively evaluate the fines incidence on the flow velocity, ad hoc large-scale experiments coupled with polydisperse simulations are required.

References

Anderson, T.B., Jackson, R., 1967. Fluid mechanical description of fluidized beds. Ind. Eng. Chem. Fundamentals 6 (4), 527–539. https://doi.org/10.1021/i160024a007.

Beetstra, R., van der Hoef, M.A., Kuipers, J.A.M., 2007. Drag force of intermediate Reynolds number flow past mono- and bidisperse arrays of spheres. AIChE J. 53 (2), 489–501. https://doi.org/10.1002/aic.11065.

Benyahia, S., Syamlal, M., O'Brien, T.J, 2006. Extension of Hill-Koch-Ladd drag correlation over all ranges of Reynolds number and solids volume fraction. Powder Technol. 162 (2), 166–174. https://doi.org/10.1016/j.powtec.2005.12.014.

Benyahia, S., Syamlal, M., & O'Brien, T.J. (2012). Summary of MFIX Equations 2012-1. Retrieved from https://mfix.netl.doe.gov/documentation/MFIXEquations2005-4-4.pdf.

Boyle, E.J., & Massoudi, M. (1989). A kinetic theory derivation of the stress tensor for granular material that includes normal stress effects. *Tech. Rep. DOE/METC-89/4088, DE89 00,977, 66 pp., U.S. Dep. of Energy, Washington, D. C.*.

Breard, E.C.P., Dufek, J., Roche, O., 2019. Continuum modeling of pressure-balanced and fluidized granular flows in 2-D: comparison with glass bead experiments and implications for concentrated pyroclastic density currents. J. Geophys. Res. 1–27. https://doi.org/10.1029/2018JB016874.

Campbell, C.S., 1990. Rapid granular flows. Annu. Rev. Fluid Mech. 22 (1), 57–90. https://doi.org/10.1146/annurev.fl.22.010190.000421.

Cleary, P.W., Sawley, M.L., 2002. DEM modelling of industrial granular flows: 3D case studies and the effect of particle shape on hopper discharge. Appl. Math. Modell. 26 (2) https://doi.org/10.1016/S0307-904X(01)00050-6, 89–11.

Cundall, P.A., Strack, O.D.L., 1979. A discrete numerical model for granular assemblies. Geotechnique 29 (1), 47–65. https://doi.org/10.1680/geot.1979.29.1.47.

Dartevelle, S., 2004. Numerical modeling of geophysical granular flows: 1. A comprehensive approach to granular rheologies and geophysical multiphase flows. Geochem., Geophys., Geosyst. 5 (8) https://doi.org/10.1029/2003GC000636.

Dartevelle, S., Rose, W.I., Stix, J., Kelfoun, K., Vallance, J.W., 2004. Numerical modeling of geophysical granular flows: 2. Computer simulations of plinian clouds and pyroclastic flows and surges. Geochem., Geophys., Geosyst. 5 (8), 1–36. https://doi.org/10.1029/2003GC000637.

Druitt, T.H., 1998. Pyroclastic density currents. Geological Society, London, Special Publications 145 (1), 145–182.

Ergun, S. (1952). Fluid flow through packed columns. *Chem. Eng. Prog.*, 48–89. https://doi.org/citeulike-article-id:7797897.

Fedors, R.F., Landel, R.F., 1979. An empirical method of estimating the void fraction in mixtures of uniform particles of different size. Powder Technol. 23 (2), 225–231. https://doi.org/10.1016/0032-5910(79)87011-4.

Garg, R., Galvin, J., Li, T., Pannala, S., 2012. Open-source MFIX-DEM software for gas-solids flows: part I-verification studies. Powder Technol. 220, 122–137. https://doi.org/10.1016/j.powtec.2011.09.019.

Gera, D., Syamlal, M., O'Brien, T.J, 2004. Hydrodynamics of particle segregation in fluidized beds. Int. J. Multiphase Flow 30 (4), 419–428. https://doi.org/10.1016/j.ijmultiphaseflow.2004.01.003.

Gidaspow, D., 1994. Continuum and kinetic theory descriptions. Multiphase Flow and Fluidization.

Hill, R.J., Koch, D.L., Ladd, A.J.C., 2001. Moderate-Reynolds-number flows in ordered and random arrays of spheres. J. Fluid Mech. 448, 243–278. https://doi.org/10.1017/s0022112001005936.

Iddir, H., Arastoopour, H., 2005. Modeling of multitype particle flow using the kinetic theory approach. AIChE J. 51 (6), 1620–1632. https://doi.org/10.1002/aic.10429.

Iverson, R.M., 1997. The physics of Debris flows. Rev. Geophys. 35 (3), 245–296. https://doi.org/10.1029/97RG00426.

Jenkins, J.T., 1992. Boundary conditions for rapid granular flow: flat, frictional walls. J. Appl. Mech., Trans. ASME. https://doi.org/10.1115/1.2899416.

Johnson, P.C., Jackson, R., 1987. Frictional-collisional constitutive relations for granular materials, with application to plane shearing. Journal of Fluid Mechanics 176, 67–93. https://doi.org/10.1017/S0022112087000570.

Le Roux, J.P., 2003. Can dispersive pressure cause inverse grading in grain flows?-discussion. Journal of Sedimentary Research 73 (2), 333–334. https://doi.org/10.1306/043002730333.

Lebowitz, J.L., 1964. Exact solution of generalized Percus-Yevick equation for a mixture of hard spheres. Phys. Rev. (A133), 895–899. https://doi.org/10.1103/PhysRev.133.A895.

Li, T., Garg, R., Galvin, J., Pannala, S., 2012. Open-source MFIX-DEM software for gas-solids flows: part II - validation studies. Powder Technol. 220, 138–150. https://doi.org/10.1016/j.powtec.2011.09.020.

Li, Tingwen, Benyahia, S., 2012. Revisiting Johnson and Jackson boundary conditions for granular flows. AIChE J. 58 (7), 2058–2068. https://doi.org/10.1002/aic.12728.

Louge, M.Y., Mastorakos, E., Jenkins, J.T., 1991. The role of particle collisions in pneumatic transport. J. Fluid Mech. 231, 345–359. https://doi.org/10.1017/S0022112091003427.

Lu, L., Xu, Y., Li, T., Benyahia, S., 2018. Assessment of different coarse graining strategies to simulate polydisperse gas-solids flow. Chem. Eng. Sci. 179, 53–63. https://doi.org/10.1016/j.ces.2018.01.003.

Lube, G., Breard, E.C., Jones, J., Fullard, L., Dufek, J., Cronin, S.J., Wang, T., 2019. Generation of air lubrication within pyroclastic density currents. Nat. Geosci. 12, 381–386.

Lube, G., Breard, E.C.P., Esposti-Ongaro, T., Dufek, J., Brand, B., 2020. Multiphase flow behaviour and hazard prediction of pyroclastic density currents. Nat. Rev. Earth Environ. 1 (7), 348–365. https://doi.org/10.1038/s43017-020-0064-8.

Lun, C.K.K., Savage, S.B., Jeffrey, D.J., Chepurniy, N., 1984. Kinetic theories for granular flow: inelastic particles in Couette flow and slightly inelastic particles in a general flowfield. J. Fluid Mech. 140, 223–256. https://doi.org/10.1017/S0022112084000586.

Mansoori, G.A., Carnahan, N.F., Starling, K.E., Leland, T.W., 1971. Equilibrium thermodynamic properties of the mixture of hard spheres. The Journal of Chemical Physics 54 (4), 1523–1526. https://doi.org/10.1063/1.1675048.

Neglia, F., Dioguardi, F., Sulpizio, R., Ocone, R., Sarocchi, D., 2022. Computational fluid dynamic simulations of granular flows: insights on the flow-wall interaction dynamics. Int. J. Multiphase Flow 157, 104281. https://doi.org/10.1016/J.IJMULTIPHASEFLOW.2022.104281.

Patwardhan, V.S., Tien, C., 1985. Sedimentation and liquid fluidization of solid particles of different sizes and densities. Chem. Eng. Sci. 40 (7), 1051–1060. https://doi.org/10.1016/0009-2509(85)85062-4.

Pritchett, J.W., Blake, T.R., Garg, S.K., 1978. A numerical model of gas fluidized beds. A. I.Ch.E. Symp. Ser. 176, 134–148.

Roche, O., Gilbertson, M.A., Phillips, J.C., Sparks, R.S.J., 2005. Inviscid behaviour of fines-rich pyroclastic flows inferred from experiments on gas-particle mixtures. Earth and Planetary Science Letters 240 (2), 401–414. https://doi.org/10.1016/j.epsl.2005.09.053.

Roche, O., Montserrat, S., Nin˜o, Y., & Tamburrino, A. (2010). Pore fluid pressure and internal kinematics of gravitational laboratory air-particle flows: Insights into the emplacement dynamics of pyroclastic flows. *Journal of Geophysical Research: Solid Earth, 115*(B9).

Rodriguez-Sedano, L.A., Sarocchi, D., Sulpizio, R., Borselli, L., Campos, G., Moreno Chavez, G., 2016. Influence of particle density on flow behavior and deposit architecture of concentrated pyroclastic density currents over a break in slope: insights from laboratory experiments. J. Volcanol. Geotherm. Res. https://doi.org/10.1016/j.jvolgeores.2016.10.017.

Sarocchi, D., Sulpizio, R., Macías, J.L., Saucedo, R., 2011. The 17 July 1999 block-and-ash flow (BAF) at Colima Volcano: new insights on volcanic granular flows from textural analysis. J. Volcanol. Geotherm. Res. 204 (1–4), 40–56. https://doi.org/10.1016/j.jvolgeores.2011.04.013.

Savage, S.B., 1998. Analyses of slow high-concentration flows of granular materials. J. Fluid Mech. 377, 1–26. https://doi.org/10.1017/S0022112098002936.

Schaeffer, D.G., 1987. Instability in the evolution equations describing incompressible granular flow. J. Differ. Equ. https://doi.org/10.1016/0022-0396(87)90038-6.

Srivastava, A., Sundaresan, S., 2003. Analysis of a frictional-kinetic model for gas-particle flow. Powder Technol. 129 (1–3), 72–85. https://doi.org/10.1016/S0032-5910(02)00132-8.

Sulpizio, R., Dellino, P., Doronzo, D.M., Sarocchi, D., 2014. Pyroclastic density currents: state of the art and perspectives. J. Volcanol. Geotherm. Res. 283, 36–65. https://doi.org/10.1016/j.jvolgeores.2014.06.014.

Sulpizio, R., Castioni, D., Rodriguez-Sedano, L.A., Sarocchi, D., Lucchi, F., 2016. The influence of slope-angle ratio on the dynamics of granular flows: insights from laboratory experiments. Bull. Volcanol. 78 (11), 1–11. https://doi.org/10.1007/s00445-016-1069-5.

Sweeney, M.R., Valentine, G.A., 2017. Impact zone dynamics of dilute mono-and polydisperse jets and their implications for the initial conditions of pyroclastic density currents. Phys. Fluids 29, 93304. https://doi.org/10.1063/1.5004197.

Syamlal, M., Ness, H., Virginia, W., & Virginia, W. (1987). *The particle-particle drag term in a multiparticle model of fluidization*. United States: N. p. Web.

Syamlal, M., O'Brien, T.J., 1988. Simulation of granular layer inversion in liquid fluidized beds. International Journal of Multiphase Flow 14 (4), 473–481. https://doi.org/10.1016/0301-9322(88)90023-7.

Syamlal, M., Rogers, W., & O`Brien, T.J. (1993). MFIX documentation theory guide. *DOE/METC-94/1004, DE9400,097. USDOE Morgantown Energy Technology Center, WV*. https://doi.org/10.2172/10145548.

Valentine, G.A., Sweeney, M.R., 2018. Compressible flow phenomena at inception of lateral density currents fed by collapsing gas-particle mixtures. J. Geophys. Res. 123 (2), 1286–1302. https://doi.org/10.1002/2017JB015129.

Valentine, G.A., 2020. Initiation of dilute and concentrated pyroclastic currents from collapsing mixtures and origin of their proximal deposits. Bull. Volcanol. 82 (2) https://doi.org/10.1007/s00445-020-1366-x.

Van Wachem, B.G.M., Schouten, J.C., Van den Bleek, C.M., Krishna, R., Sinclair, J.L., 2001. Comparative analysis of CFD models of dense gas-solid systems. AIChE J. 47 (5), 1035–1051. https://doi.org/10.1002/aic.690470510.

Wen, C.Y., Yu, Y.H., 1966. Mechanics of fluidization. Chem. Eng. Prog., Symp. Ser. 62–100.

Yu, A.B., Standish, N., 1987. Porosity calculations of multi-component mixtures of spherical particles. Powder Technol. 52, 233–241. https://doi.org/10.1016/0032-5910(87)80110-9.